Ground State Structures of $Fe_2O_{4-6}^+$ Clusters Probed by Reactions with N_2

Wei Xue,[†,‡] Shi Yin,[†,‡] Xun-Lei Ding,[†] Sheng-Gui He,*[,†] and Mao-Fa Ge*[,†]

Beijing National Laboratory for Molecular Sciences (BNLMS), State Key Laboratory for Structural Chemistry of Unstable and Stable Species, Institute of Chemistry, Chinese Academy of Sciences, Beijing 100190, China, and Graduate University of the Chinese Academy of Sciences, Beijing 100039, China

Received: November 27, 2008; Revised Manuscript Received: March 20, 2009

Reactions of small cationic iron oxide clusters ($Fe_2O_{4-6}^+$) with N_2 are investigated by experiments and first principle calculations. The cationic iron oxide clusters are generated by reaction of laser ablated iron plasma with O_2 in a supersonic expansion, and are reacted with N_2 in a fast flow reactor at near room temperature conditions. Cluster cations are detected by a time-of-flight mass spectrometer. The substitution reaction $Fe_2O_n^+ + N_2 \rightarrow Fe_2O_{n-2}N_2^+ + O_2$ is observed for $n = 5$ but not for $n = 4$ and 6. Density functional theory calculations predict that the low-lying energy structures of $Fe_2O_{4-6}^+$ are with side-on (η^1-O_2) or end-on (η^2-O_2) bonded molecular oxygen unit(s). The calculations further predict that the substitution of η^1-O_2 and η^2-O_2 in $Fe_2O_{4,6}^+$ clusters by N_2 is exothermic and subject to negative and positive overall reaction barriers, respectively, at room temperature. We thus propose that the ground state structures of $Fe_2O_4^+$ and $Fe_2O_6^+$ contain η^2-O_2. In contrast, both the experiment and theory favor a η^1-O_2 in the ground state structure of $Fe_2O_5^+$.

1. Introduction

The bonding of O_2 to transition metal has been of interest for a long period of time because of the biological and industrial importance of oxygen activation by metals, especially by iron.[1] The common modes of O_2 binding to iron are end-on (superoxo-, denoted as η^1-O_2), side-on (peroxo-, denoted as η^2-O_2), and inserted (oxo-).[2] Well-controlled studies on small iron oxide clusters provide a convenient avenue to obtain detailed information about the interaction between oxygen and iron. Tremendous research efforts have been devoted to studying the structures and properties of monoiron oxide clusters by using methods of matrix isolation spectroscopy, photoelectron spectroscopy (PES), mass spectrometry, theoretical calculations, and so on.[2−17] Even so, the ground state structures of some small oxygen-rich iron oxide clusters, such as FeO_4,[4−15] are still not well-determined. Although there are many reports that the (η^2-O_2)FeO_2 with a nonplanar C_{2v} symmetry is the ground state structure of FeO_4,[4−8] the structure with T_d symmetry is predicted to be slightly more stable than (η^2-O_2)FeO_2 in some other studies.[9−11]

Compared to the tremendous efforts on monoiron oxides, structures and properties of diiron oxide clusters are relatively less studied. Diiron oxo complexes are a common structural motif in a class of metalloproteins and methane oxygenases, and research on them has become one hotspot in biochemistry.[18] Meanwhile, researchers are interested in studies of the structures and properties of diiron oxide clusters, such as Fe_2O_2, which has a diamond core structure and is thought to be the structure for the key intermediate in the methane monooxygenase catalytic cycle.[19]Fe_2O_2 has been exclusively studied in the isolated form.[4,5,11−14,20] Several other diiron oxide molecules in different charge states have also been studied.[4,5,11−14,21−25] Wu et al.[5] studied the bonding properties of $Fe_2O_{1-5}^-$ and Fe_2O_{1-5} by PES a decade ago. Shiroishi et al.[11,12] studied the structural and magnetic properties of $Fe_2O_{1-5}^-$ and Fe_2O_{1-6} by first principle calculations. Schröder et al.[22] and Molek et al.[26] studied the structures of diiron oxide cations using collision-induced dissociation (CID on $Fe_2O_{1-3}^+$) and photodissociation (PD on $Fe_2O_{2-6}^+$ and $Fe_2O_8^+$) mass spectrometry, respectively. Reddy et al.[23,24] theoretically studied the chemical reactivity of the Fe_2O_3 cluster toward CO. By using mass spectrometry and first principle calculations, Reilly et al.[13,14] studied CO oxidation by $Fe_2O_{1-5}^+$ and $Fe_2O_{3-6}^-$ and we[27] studied the same oxidation by Fe_2O_{3-5}.

In spite of the extensive studies mentioned above, understanding the structures and properties of small diiron oxide clusters in different charge states is far from complete. For instance, the ground state structure of a certain cluster, e.g., Fe_2O_3, is not definitely determined. Wu et al.[5] and Reddy et al.[24] predicted a distorted triangular bipyramid structure for Fe_2O_3, while Shiroishi et al.[11] and we[27] predicted a structure with an Fe−O−Fe−O four-membered ring plus an O atom doubly bonded with one of the iron atoms. The CID and PD experiments (loss of O_2 from $Fe_2O_{3-6}^+$ upon collision or photon absorption)[14,22,27] suggest that $Fe_2O_{3-6}^+$ clusters may contain O−O unit(s) whereas the first principle calculations[14] predict that none of these clusters has an O−O unit. It should be pointed out that the calculations in ref 14 do not disagree with the CID or PD experiments since the calculated thermodynamics shows that the O_2 loss is less endothermic than the O loss for $Fe_2O_{3-6}^+$ clusters. Considering that possible kinetic barriers can make O_2 loss more difficult than O loss for iron oxide clusters without O−O moiety, the structures of $Fe_2O_{3-6}^+$ have not been definitely determined. We try to readdress the structures of $Fe_2O_{4-6}^+$ in this study.

Vibrational spectroscopy studies such as those carried out on gas phase[28] or matrix isolated species[29] are well-known experimental approaches to obtain firm structural information. However, vibrational spectra of $Fe_2O_{4-6}^+$ have not been reported. Anion PES is a valuable method to probe the bonding and structural properties of anionic and neutral clusters.[5,30] Although the structures of $Fe_2O_{4-5}^-$ have been well probed (and to have no O−O unit),[5] it is still necessary to obtain structural

* To whom correspondence should be addressed. E-mail: shengguihe@iccas.ac.cn and gemaofa@iccas.ac.cn. Fax: +86-10-62559373.
† Chinese Academy of Sciences.
‡ Graduate University of the Chinese Academy of Sciences.

10.1021/jp810426s CCC: $40.75
Published on Web 04/07/2009

information directly for cations because additional charge(s) may change a cluster structure significantly. Cluster reactivity toward a suitable (probe) molecule may also be used to obtain firm structural information since the reactivity depends heavily on the bonding and structural properties.[27] In this study, we use this "molecular probe" method combined with quantum chemistry calculations to study the structures of $Fe_2O_{4-6}^+$ clusters.

2. Methods

The experiments performed in this study are conducted with a TOF-MS coupled with a laser ablation/supersonic expansion cluster source and a fast flow reactor.[31] The design of the apparatus is similar to the one described in refs 27 and 32. The vacuum system of the apparatus consists of two chambers. One of the chambers is used for cluster generation/reaction and the other is for cluster ion detection. The two chambers are connected through a 5 mm diameter skimmer. The iron oxide clusters are generated by the reaction of laser ablation generated iron plasmas with O_2 seeded (0.5%) in the helium carrier gas. The typical backing pressure of the He gas is 5 atm. To generate the iron plasmas, a Nd:YAG laser beam (532 nm, 5 mJ/pulse, 8 ns duration, 10 Hz) is focused onto an iron metal disk (15 mm diameter, 0.13 mm thickness, 99.7% purity from Aldrich). The disk is rotated and translated to continually expose a fresh surface. The carrier gas seeded with O_2 is controlled by a first pulsed valve (General Valve, series 9). The clusters are formed in a narrow cluster formation channel (2 mm inner diameter (i.d.)) that contains a waiting room (3 mm i.d.). The lengths of the channel and the waiting room are adjustable to optimize the cluster growth conditions. The typical lengths used are 1 cm for the waiting room and 2 cm for the rest of the channel. A fast flow reactor with 6 mm i.d. and 8 cm length is coupled with the narrow cluster formation channel. The generated iron oxide cluster cations react with reactant molecules (N_2, CO, NO, etc.) seeded in argon carrier gas that is controlled by a second pulsed valve. The amount of gas pulsed into the chamber by the first valve is about 80 times that of the gas pulsed by the second valve. Durations of the two gas pulses are about the same ($\sim$250 μs) in this study. The instantaneous gas pressure in the fast flow reactor is about 5 Torr and the possible reactions take place at near ambient ($\sim$298 K) temperature. The reactant and product ions enter the second chamber for the TOF detection. The synchronization of laser firing, pulsed valve openings, and ion detection is managed through commercially available and homemade electronics. The mass signal is generated by a dual microchannel plate detector and recorded with a digital acquisition card that is controlled by a Labview based program.

The calculations are performed by the Gaussian 03 program,[33] using density functional theory (DFT) with the hybrid B3LYP exchange-correlation functional.[34] Note that energetics, bond lengths, and vibrational frequencies of the ground and low lying excited states of Fe_2, Fe_2^-, and FeO^+ are found to be best described by the B3LYP functional after an examination of a number of different types of generalized gradient approximation (GGA) functionals (straight GGA, hybrid GGA, meta-GGA, and hybrid meta-GGA) by Sorkin et al.[35] The basis set adopted is the triply split 6-311+G* basis set with one set of diffuse and polarization functions for all of the atoms.[36] In this study, the B3LYP/6-311+G* calculations are performed to study the structures and energies of $Fe_2O_{2-6}^+$ and $Fe_2O_5^-$ clusters as well as the reaction pathways of $Fe_2O_{4-6}^+$ with N_2. The reaction pathway calculations involve the geometry optimizations of reaction intermediates and transition states. The transition state optimizations are performed by using either the Berny algorithm[37] or the synchronous transit-guided quasi-Newton (STQN) method.[38] The vibrational frequency calculations are performed to check that the reaction intermediates and species in the transition states have zero and one imaginary frequency, respectively. The intrinsic reaction coordinate (IRC) calculations[39] are performed to check that a transition state connects two appropriate local minima in the reaction pathways. The energies reported in this study are zero-point corrected energies (ΔH_{0K}) or free energies of formation at 298.15 K (ΔG_{298K}). Cartesian coordinates, energies, and vibrational frequencies for all of the optimized structures are listed as tables in the Supporting Information.

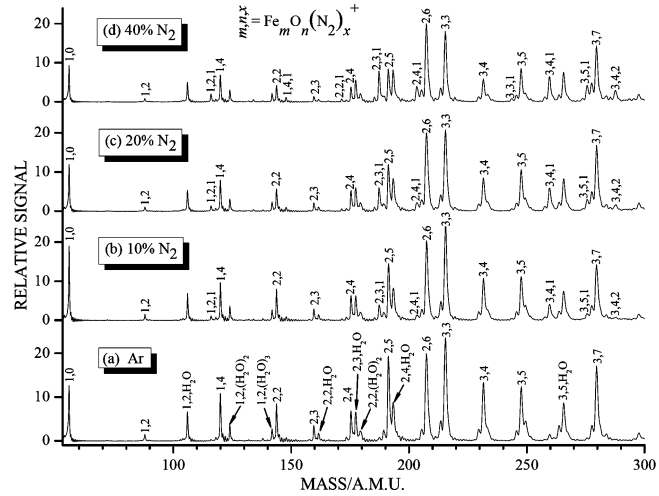

Figure 1. TOF mass spectra for reaction of $Fe_mO_n^+$ ($m \leq 3$) clusters with N_2 in the fast flow reactor. The N_2 concentrations are 0% (a), 10% (b), 20% (c), and 40% (d) seeded in the argon carrier gas. Note that the weak side or shoulder peaks at the low-mass side of the main peaks are due to ^{54}Fe isotopomers.

3. Results

3.1. Experimental Results. Figure 1 plots the TOF mass spectra for collisions/reactions of the preformed $Fe_mO_n^+$ ($m \leq 3$) with different concentrations of N_2 seeded in Ar in the fast flow reactor. N_2 is usually chemically inert; however, the collisions of N_2 with cationic iron oxide clusters produce N_2 containing products $Fe_mO_nN_2^+$ and $Fe_3O_4N_4^+$. Among the generated $Fe_{1-3}O_n^+$ clusters in Figure 1, $Fe_2O_5^+$ and $Fe_3O_4^+$ have relatively high reactivity toward N_2. Signals of $Fe_2O_5^+$ and $Fe_3O_4^+$ decrease by about a factor of 2 as the N_2 concentration increases from 0 to 40%. Reaction of $Fe_3O_4^+$ with N_2 can produce primary and secondary addition products $Fe_3O_4N_2^+$ and $Fe_3O_4N_4^+$, respectively. This interpretation is supported by the observation that as the N_2 concentration increases, the magnitude of the signal increase of the product ions (mainly $Fe_3O_4N_2^+$) is about the same as the magnitude of the signal decrease of the reactant ions ($Fe_3O_4^+$). Although $Fe_2O_5^+$ is also quite reactive toward N_2, the corresponding association product $Fe_2O_5N_2^+$ is not observed. Among the observed products ($Fe_2O_{2-4}N_2^+$) that can be produced from reactions of $Fe_2O_{2-6}^+$ with N_2, $Fe_2O_3N_2^+$ has the strongest signal and its signal magnitude is significantly greater than the magnitude of signal decrease of $Fe_2O_3^+$. In addition, $Fe_2O_4N_2^+$ can be interpreted as the association product of $Fe_2O_4^+$ with N_2 and $Fe_2O_6^+$ is not reactive toward N_2 within the experimental uncertainty (10% for intensities of the mass peaks). A consistent conclusion is that the reaction of $Fe_2O_5^+$ with N_2 produces

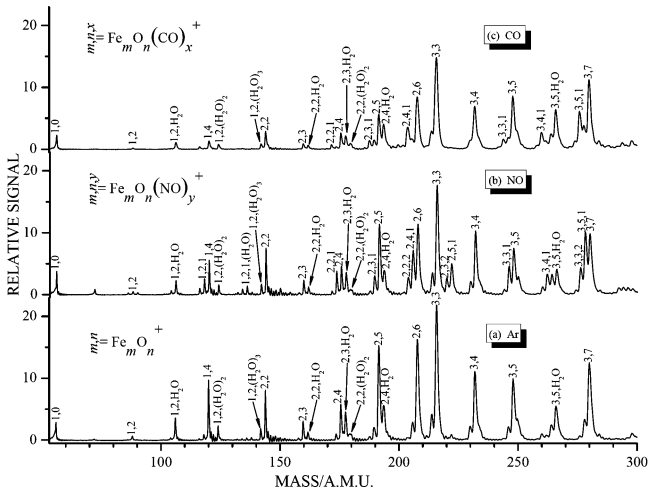

Figure 2. TOF mass spectra for reaction of $Fe_mO_n^+$ ($m \leq 3$) clusters with NO or CO in the fast flow reactor. Note that the weak side or shoulder peaks at the low-mass side of the main peaks are due to ^{54}Fe isotopomers.

$Fe_2O_3N_2^+$. The mechanism is assumed to be a simple substitution reaction: $Fe_2O_5^+ + N_2 \rightarrow Fe_2O_3N_2^+ + O_2$.

Reactions of $Fe_mO_n^+$ with other gas molecules (O_2, CO, NO, etc.) in the fast flow reactor also have been studied. No relative signal change of the preformed iron oxide clusters and no product clusters are observed in the reaction with O_2. So these clusters are inert toward O_2 under our experimental conditions. The cluster cations are generally much more reactive toward CO and NO (Figure 2) than toward N_2 (Figure 1) because only 1% CO and NO in Ar can cause a significant change of the mass signals and some products $Fe_mO_nCO^+$ and $Fe_mO_nNO^+$ are apparently observed. $Fe_2O_6^+$ is not reactive toward N_2 (Figure 1). In contrast, $Fe_2O_6^+$ becomes reactive when CO and NO are used as reactants.

3.2. Computational Results. ***3.2.1. Accuracy of the Calculations.*** To gauge the accuracy of the computations under the B3LYP/6-311+G* level of theory, the calculated ionization and bond dissociation energies of iron oxides and related species are compared with available experimental data[2,40−49] (see Table 1). The calculated values from a pure GGA functional proposed by Perdew, Burke, and Ernzerhof (PBE)[50] are also listed for comparison. Considering a large experimental uncertainty for ionization energy (IE) of FeO_2, both the B3LYP and PPE functionals have reasonably good performance for the IEs of FeO_{0-2}. As for the bond energies (D), the B3LYP generally has much better performance than the PBE does. The PBE calculations overestimate the experimentally well-determined D values of O_2, CO_2, FeO, and FeO^+ by 0.8−1.3 eV, whereas the B3LYP can predict these D values with good (for O_2, CO_2, and FeO) or reasonably good (for FeO^+) accuracy. The experimental D values of iron dioxides ($FeO_2^{0/+}$) have not been very well determined in the literature. An indirect but reliable experimental determination of $D(Fe^+-O_2)$ can be found in ref 2, where the ligand exchange experiments were performed to bracket $D(Fe^+-O_2)$. The $D(Fe^+-O_2)$ is found to be between the known D values of $Fe^+-C_3H_8$ and Fe^+-CO/H_2O. The B3LYP calculations agree well with the ligand exchange experiments for $D(Fe^+-O_2)$, while the PBE again overestimates this value by 0.87 eV. The experimental D values of FeO^+-O and FeO−O can be determined from $D(Fe^+-O_2)$ and related ionization and bond energies (see footnotes f and g of Table 1). If $D(Fe^+-O_2)$ determined from the ligand exchange experiments is used, $D(FeO^+-O) = 2.70 \pm 0.28$ eV and $D(FeO-O) = 3.64 \pm 0.57$ eV can be obtained. These two values are very well reproduced by the B3LYP calculations. The PBE functional overestimates the above $D(FeO^+-O)$ and $D(FeO^+-O)$ by 0.9 and 1.4 eV, respectively. The B3LYP and PBE show similar performance for D values of oxygen poor species Fe_2-O and Fe_2^+-O. The experimental $D(Fe_2O^+-O)$ is very well predicted by the B3LYP while the PBE overestimates $D(Fe_2O^+-O)$ by 1.2 eV. The D values of Fe^+-N can be reasonably predicted by the B3LYP calculations. One may conclude that the bond energies of iron oxides can be reasonably predicted by the B3LYP functional while the PBE generally overestimates all of them by about 1 eV.

3.2.2. Structures and Energetics. Figure 3 shows the lowest energy isomers for $Fe_2O_{2-6}^+$ clusters. The ground state of $Fe_2O_2^+$ has a four-membered-ring structure (Fe−O−Fe−O). This ring moiety exists in all of the DFT calculated ground state structures of larger clusters ($Fe_2O_{3-6}^+$). Two structural isomers of the $Fe_2O_3^+$ cluster are tested. The Fe−O−Fe−O ring based structure ($Fe_2O_3^+$/C1) is more stable than the *open* structure ($Fe_2O_3^+$/C2). Among the three isomers of $Fe_2O_4^+$, $Fe_2O_4^+$/C3, which has two terminal Fe−O bonds, is above the ground state isomer by 1.55 eV. A η^2-O_2 exists in the ground state of $Fe_2O_4^+$ ($Fe_2O_4^+$/C1) while the structure ($Fe_2O_4^+$/C2) with a η^1-O_2 is above the ground state by only 0.26 eV. The ground state structure of $Fe_2O_5^+$ consists of $Fe_2O_3^+$/C1 and a η^1-O_2. Unlike $Fe_2O_4^+$, $Fe_2O_5^+$ with a η^2-O_2 moiety ($Fe_2O_5^+$/C2) is not the ground state. The $Fe_2O_3^+$/C2 based structural isomers of $Fe_2O_5^+$ (C3 and C4) are slightly higher in energy than the ground state. Similar to the $Fe_2O_3^+$/C1 based isomers of $Fe_2O_5^+$ (C1 and C2), the structure $Fe_2O_5^+$/C4 with a η^2-O_2 moiety is higher in energy than $Fe_2O_5^+$/C3 with a η^1-O_2 moiety. The structure isomer of $Fe_2O_5^+$ (C5) with three terminal Fe−O bonds is above the ground state by 1.60 eV. The ground state structure of $Fe_2O_6^+$ consists of $Fe_2O_4^+$/C1 and a η^2-O_2. Unlike $Fe_2O_5^+$ but similar to $Fe_2O_4^+$, $Fe_2O_6^+$ with a η^1-O_2 moiety ($Fe_2O_6^+$/C2) is not the ground state. The structure isomer of $Fe_2O_6^+$ (C3) with four terminal Fe−O bonds is very high in energy compared with the structures ($Fe_2O_6^+$/C1 and C2) with $\eta^{1/2}$-O_2 moieties.

The binding energies of O_2 with related $Fe_2O_{2-4}^+$ species are listed in Table 2. The binding energies range from 0.4 to 0.7 eV, which indicates that the O−O moiety is weakly bonded in $Fe_2O_{4-6}^+$. The binding energies of N_2 with corresponding $Fe_2O_{2-4}^+$ species are also given in Table 2. The binding between $Fe_2O_{2-4}^+$ and N_2 is always stronger than that between $Fe_2O_{2-4}^+$ and O_2, which indicates than the substitution reaction of $Fe_2O_{4-6}^+ + N_2 \rightarrow Fe_2O_{2-4}N_2^+ + O_2$ is exothermic.

3.2.3. Reactions of $Fe_2O_{4-6}^+$ with N_2. Table 1 shows that the B3LYP/6-311+G* calculations are in generally good agreement with the experimental measurements of bond energies of iron oxides and oxygen molecule. The structures of $Fe_2O_4^+$/C3, $Fe_2O_5^+$/C5, and $Fe_2O_6^+$/C3 without the O−O moiety are significantly (more than 1.3 eV) higher in energy than the structures with one or two O−O moieties (Figure 3). It may be safe to discard the possibility that $Fe_2O_4^+$/C3, $Fe_2O_5^+$/C5, or $Fe_2O_6^+$/C3 is the ground state of the diiron oxide cluster. However, the DFT calculations may not be accurate enough to differentiate the relative energies of structures with η^1-O_2 and η^2-O_2 moieties (such as $Fe_2O_{4-6}^+$/C1 versus $Fe_2O_{4-6}^+$/C2) that are close in energy within 0.09−0.26 eV. The N_2 substitution reactions of $Fe_2O_{4-6}^+ + N_2 \rightarrow Fe_2O_{2-4}N_2^+ + O_2$ that are all exothermic (Table 2) may be used to probe how O−O is bonded in the $Fe_2O_{4-6}^+$ clusters.

Figures 4−6 plot the DFT calculated pathways of reactions $Fe_2O_n^+$/C1/C2 + $N_2 \rightarrow Fe_2O_{n-2}N_2^+ + O_2$ for $n = 4-6$,

TABLE 1: Comparison of DFT Calculated and Experimental Ionization and Bond Dissociation Energies

	ionization or dissociation energies (IE or *D*)/eV			
	calcd		exptl	
reactions[a]	B3LYP[b]	PBE[c]	energies	ref
$^5Fe \rightarrow {}^4Fe^+ + e$	7.792	7.85	7.9023 ± 0.0001	40
$^5FeO \rightarrow {}^6FeO^+ + e$	8.856	8.8	8.56 ± 0.01	41
$^5FeO_2 \rightarrow {}^6FeO_2^+ + e$	9.640	10.23	9.5 ± 0.5	42
$^3O_2 \rightarrow {}^3O + {}^3O$	5.087	6.20	5.115 ± 0.001	43
$^1CO_2 \rightarrow {}^1CO + {}^3O$	5.479	6.34	5.543 ± 0.002	44
$^5FeO \rightarrow {}^5Fe + {}^3O$	4.251	5.51	4.18 ± 0.01	45
$^6FeO^+ \rightarrow {}^4Fe^+ + {}^3O$	3.187	4.57	3.52 ± 0.02	41
$^6FeO_2^+ \rightarrow {}^4Fe^+ + {}^3O_2$	0.975	1.98	1.11 ± 0.28	2[d]
			2.0 ± 0.5	46[e]
$^6FeO_2^+ \rightarrow {}^6FeO^+ + {}^3O$	2.874	3.61	2.70 ± 0.28	b[f]
$^5FeO_2 \rightarrow {}^5FeO + {}^3O$	3.659	5.05	3.64 ± 0.57	b[g]
			4.46 ± 0.22	42
			4.54 ± 0.20	47
$^9Fe_2O \rightarrow {}^9Fe_2 + {}^3O$	6.098	5.97	>4.84	46
$^{10}Fe_2O^+ \rightarrow {}^8Fe_2^+ + {}^3O$	5.659	5.64	5.15 ± 0.05	46
$^{10}Fe_2O_2^+ \rightarrow {}^{10}Fe_2O^+ + {}^3O$	4.297	5.47	4.25 ± 0.27	48[h]
$^3FeN^+ \rightarrow {}^4Fe^+ + {}^4N$	2.096		2.55 ± 0.22	49

[a] Superscripts indicate the spin multiplicities (*M*) of species in the ground states determined by B3LYP/6-31+G* calculations. PBE functional may predict different *M* values for the ground state iron oxides. [b] This work. [c] Cited from ref 14. [d] The ligand exchange experiments in ref 2 determined that the binding energy of Fe^+-O_2 is greater than that of $Fe^+-C_3H_8$ (0.824 eV) and less than that of Fe^+-CO or Fe^+-H_2O (1.388 eV). [e] Calculated as $D^0(Fe^+-O_2) = D^0(Fe-O_2) + IE(Fe) - IE(FeO_2)$ in ref 46, where $D^0(Fe-O_2) = 3.6 \pm 0.1$ eV (ref 47), IE(Fe) = 7.90 eV, and $IE(FeO_2) = 9.5 \pm 0.5$ eV (ref 42). [f] Calculated as $D(FeO^+-O) = D(Fe^+-O_2) + D(O-O) - D(Fe^+-O)$, where $D(Fe^+-O_2) = 1.11 \pm 0.28$ eV, $D(O-O) = 5.115 \pm 0.001$ eV, and $D(Fe^+-O) = 3.52 \pm 0.02$ eV. [g] Calculated as $IE(FeO_2) + D(FeO^+-O) - IE(FeO)$, where $IE(FeO_2) = 9.5 \pm 0.5$ eV, $D(FeO^+-O) = 2.70 \pm 0.28$ eV, and IE(FeO) = 8.56 ± 0.01 eV. [h] From the $D(Fe_2^+-2O) = 9.40 \pm 0.27$ eV in ref 48. $D(Fe_2O^+-O)$ can be calculated as $D(Fe_2^+-2O) - D(Fe_2^+-O) = 9.40 - 5.15 = 4.25$ eV.

respectively. Reaction pathways for $Fe_2O_5^+$/C3/C4 + $N_2 \rightarrow Fe_2O_3N_2^+ + O_2$ are given in Figure 7. Reactions of $Fe_2O_{4-6}^+$/C1/C2 with N_2 are subject to negative and positive overall reaction barriers for the η^1-O_2 and η^2-O_2 containing clusters, respectively. The nonreactivity of $Fe_2O_6^+$ with N_2 by the experiments (Figure 1) can be well interpreted (Figure 6) if the true ground state of $Fe_2O_6^+$ contains no η^1-O_2. We thus propose that the true ground state of $Fe_2O_6^+$ contains two η^2-O_2 moieties (Figure 3, $Fe_2O_6^+$/C1). The structure of $Fe_2O_6^+$ is based on that of $Fe_2O_4^+$, i.e., it is reasonable that the ground state of $Fe_2O_4^+$ contains a η^2-O_2 rather than a η^1-O_2. $Fe_2O_4^+$ is not very reactive toward N_2 by the experiments (Figure 1), which also suggests that the ground state of $Fe_2O_4^+$ contains a η^2-O_2 because Figure 4 shows that $Fe_2O_4^+$ with a η^1-O_2 should be very reactive toward N_2 substitution.

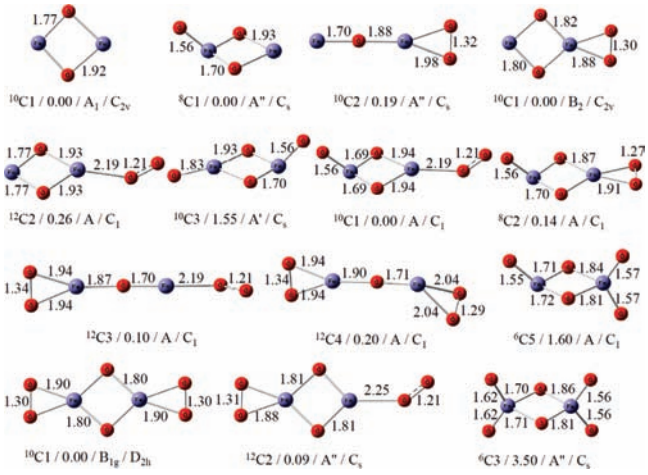

Figure 3. The lowest energy isomers of $Fe_2O_n^+$ ($2 \le n \le 6$) clusters. The spin multiplicity (*M*), the relative zero-point corrected energy (ΔH_{0K} in eV), electronic configuration (Γ), and the point group (PG) of the conformers (C*n*) are given as ^{M}C*n*/ΔH_{0K}/Γ/PG. The bond lengths are given in angstroms.

TABLE 2: Binding Energies (ΔH_{0K}) of O_2 and N_2 with Related Species in $Fe_2O_{4-6}^+$

no.	reaction[a]	ΔH_{0K}/eV
1	$Fe_2O_4^+/{}^{10}C1 \rightarrow Fe_2O_2^+/{}^{10}C1 + {}^3O_2$	0.677
2	$Fe_2O_4^+/{}^{12}C2 \rightarrow Fe_2O_2^+/{}^{10}C1 + {}^3O_2$	0.415
3	$Fe_2O_5^+/{}^{10}C1 \rightarrow Fe_2O_3^+/{}^8C1 + {}^3O_2$	0.507
4	$Fe_2O_5^+/{}^8C2 \rightarrow Fe_2O_3^+/{}^8C1 + {}^3O_2$	0.368
5	$Fe_2O_5^+/{}^{12}C3 \rightarrow Fe_2O_3^+/{}^{10}C2 + {}^3O_2$	0.606
6	$Fe_2O_5^+/{}^{12}C4 \rightarrow Fe_2O_3^+/{}^{10}C2 + {}^3O_2$	0.499
7	$Fe_2O_6^+/{}^{10}C1 \rightarrow Fe_2O_4^+/{}^{10}C1 + {}^3O_2$	0.531
8	$Fe_2O_6^+/{}^{12}C2 \rightarrow Fe_2O_4^+/{}^{10}C1 + {}^3O_2$	0.446
9	$^{10}(\eta^1\text{-}N_2)(Fe_2O_2^+/{}^{10}C1) \rightarrow Fe_2O_2^+/{}^{10}C1 + {}^1N_2$	0.753
10	$^8(\eta^1\text{-}N_2)(Fe_2O_3^+/{}^8C1) \rightarrow Fe_2O_3^+/{}^8C1 + {}^1N_2$	0.829
11	$^{10}(\eta^1\text{-}N_2)(Fe_2O_3^+/{}^{10}C2) \rightarrow Fe_2O_3^+/{}^{10}C2 + {}^1N_2$	0.888
12	$^{10}(\eta^1\text{-}N_2)(Fe_2O_4^+/{}^{10}C1) \rightarrow Fe_2O_4^+/{}^{10}C1 + {}^1N_2$	0.604
13	$Fe_2O_3^+/{}^8C1 \rightarrow Fe_2O_2^+/{}^{10}C1 + {}^3O$	2.470

[a] See Figures 3−7 for structural isomers.

The experiments indicate that $Fe_2O_5^+$ is quite reactive toward N_2 substitution $Fe_2O_5^+ + N_2 \rightarrow Fe_2O_3N_2^+ + O_2$ (Figure 1). This is supported by the DFT calculated results (Figures 5 and 7) that the substitution reactions of $Fe_2O_5^+$/C1−C4 with N_2 are subject to negative or small positive (0.12 eV) overall barriers. The DFT calculations predict that the $Fe_2O_5^+$ isomer with η^1-O_2 is more stable than the isomer with η^2-O_2 ($Fe_2O_5^+$/C1 versus C2 and $Fe_2O_5^+$/C3 versus C4 in Figure 3) and the former is more reactive than the latter toward N_2 (Figures 5 and 7). We conclude that both the experiment and theory favor a η^1-O_2 in the ground state structure of $Fe_2O_5^+$ although the possibility of a η^2-O_2 in the $Fe_2O_5^+$ ground state cannot be definitely excluded. It is noticeable that the DFT calculations (Figure 3) in this study are most probably correct in predicting how the O−O unit(s) is bonded (η^1-O_2 or η^2-O_2) in the ground states of $Fe_2O_{4-6}^+$ clusters.

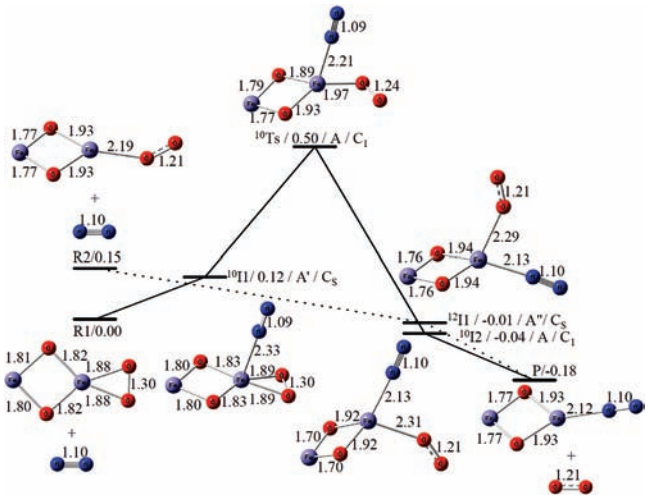

Figure 4. DFT calculated reaction pathways for $Fe_2O_4^+(^{10}B_2)$ + $N_2(^1\Sigma_g^+)$ → $Fe_2O_2N_2^+(^{10}A')$ + $O_2(^3\Sigma_g^-)$ (solid line) and $Fe_2O_4^+(^{12}A)$ + $N_2(^1\Sigma_g^+)$ → $Fe_2O_2N_2^+(^{10}A')$ + $O_2(^3\Sigma_g^-)$ (dotted line). The reaction intermediates and transition states are denoted as ^{M}I*n* and ^{M}Ts*n*, respectively, where the superscript indicates the spin multiplicities. The relative Gibbs free energy at 298.15 K (ΔG_{298K} in eV), electronic configuration (Γ), and the point group (PG) of the species are given as ΔG_{298K}/Γ/PG. The bond lengths are given in angstroms. All of the energies are relative to the total free energy of $Fe_2O_4^+(^{10}B_2)$ and $N_2(^1\Sigma_g^+)$.

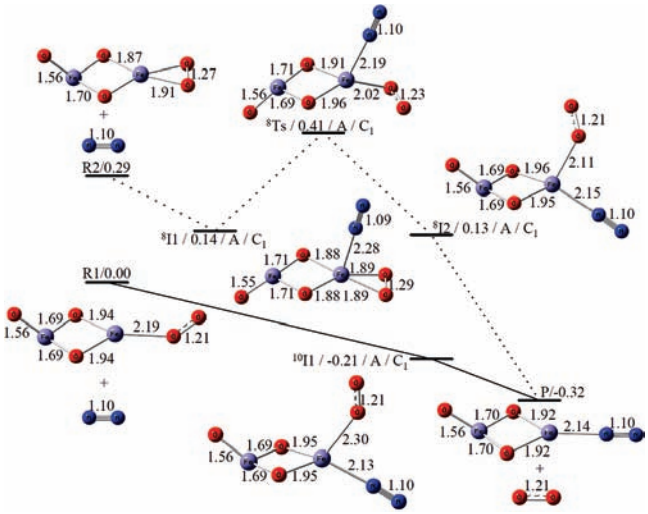

Figure 5. DFT calculated reaction pathways for $Fe_2O_5^+(^8A)$ + $N_2(^1\Sigma_g^+)$ → $Fe_2O_3N_2^+(^8A'')$ + $^3O_2(^3\Sigma_g^-)$ (dotted line) and $Fe_2O_5^+(^{10}A)$ + $N_2(^1\Sigma_g^+)$ → $Fe_2O_3N_2^+(^8A'')$ + $^3O_2(^3\Sigma_g^-)$ (solid line). See the caption of Figure 4 for explanations. All of the energies are relative to the total free energy of $Fe_2O_5^+(^{10}A)$ and $N_2(^1\Sigma_g^+)$.

4. Discussion

4.1. Comparison with Previous Results. The ground state structures of $Fe_2O_{4-6}^+$ determined in this study are very different from those in the literature.[14] The B3LYP calculations predict that the η^1-O_2 or η^2-O_2 moiety exists in the ground states of $Fe_2O_{4-6}^+$ whereas the O−O bond is broken (like $Fe_2O_{4,6}^+$/C3 and $Fe_2O_5^+$/C5 in Figure 3) under the PBE calculations in ref 14. The reason can be traced back to the differences of the iron−oxygen and oxygen−oxygen bond energies (Table 1) predicted by different functionals. The PBE overestimates energies of both iron−oxygen and oxygen−oxygen bonds by typically 1 eV. As a result, formation of two separate iron−oxygen bonds from one O_2 molecule and appropriate iron site(s) is favored by the PBE calculations. In contrast, the

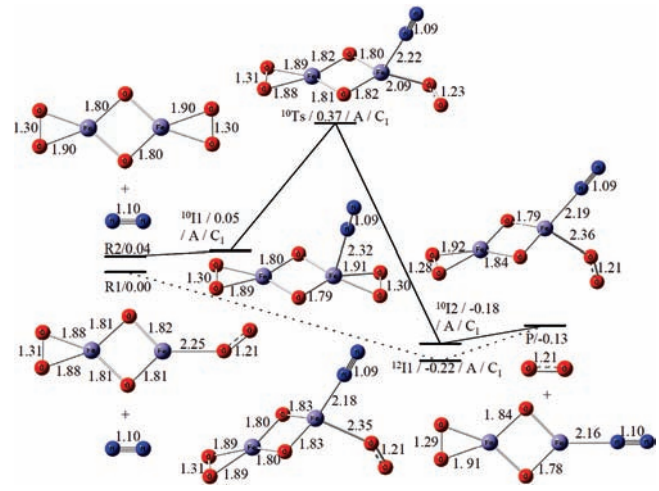

Figure 6. DFT calculated reaction pathways for $Fe_2O_6^+(^{10}B_1{}_g)$ + $^1N_2(^1\Sigma_g^+)$ → $Fe_2O_4N_2^+(^{10}A'')$ + $^3O_2(^3\Sigma_g^-)$ (solid line) and $Fe_2O_6^+(^{12}A'')$ + $^1N_2(^1\Sigma_g^+)$ → $Fe_2O_4N_2^+(^{10}A'')$ + $^3O_2(^3\Sigma_g^-)$ (dotted line). See the caption of Figure 4 for explanations. All of the energies are relative to the total free energy of $Fe_2O_6^+(^{12}A'')$ and $N_2(^1\Sigma_g^+)$.

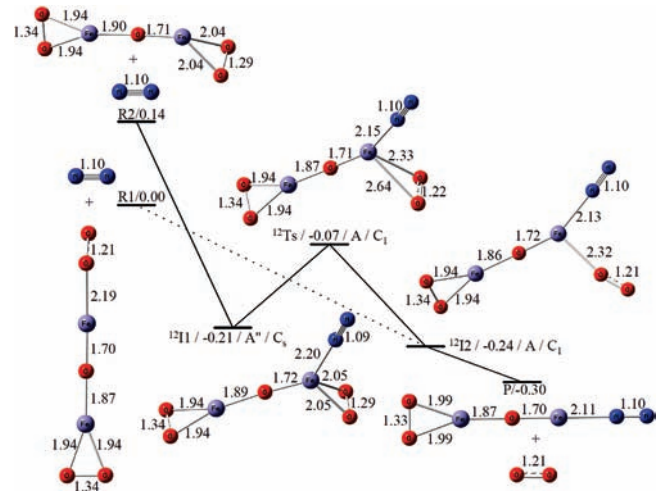

Figure 7. DFT calculated reaction pathways for $Fe_2O_5^+(^{12}A)$ (C3) + $N_2(^1\Sigma_g^+)$ → $Fe_2O_3N_2^+(^8A'')$ + $^3O_2(^3\Sigma_g^-)$ (dotted line) and $Fe_2O_5^+(^{12}A)$ (C4) + $N_2(^1\Sigma_g^+)$ → $Fe_2O_3N_2^+(^8A'')$ + $^3O_2(^3\Sigma_g^-)$ (solid line). See the caption of Figure 4 for explanations. All of the energies are relative to the total free energy of $Fe_2O_5^+(^{12}A)$ (C3) and $N_2(^1\Sigma_g^+)$.

B3LYP calculations are generally in good agreement with the experimental measurements of the iron−oxygen and oxygen−oxygen bond energies. As a result, the structures predicted by B3LYP are more reliable than those by PBE.

The experiments in this study and those in refs 14 and 26 support or are supported by the results that the O−O moiety exists in the ground state of $Fe_2O_{4-6}^+$ clusters. The reactions of CO and N_2 with mass selected $Fe_2O_{4,5}^+$ clusters at near thermal collisional energy [note that a portion of the clusters were measured to have up to 1.6 eV center-of-mass collisional energy (E_k)] were studied by Reilly et al.[14] $Fe_2O_2^+$ and $Fe_2O_3^+$ are observed as products in the reactions of $Fe_2O_4^+$ + N_2 and $Fe_2O_5^+$ + N_2, respectively. The calculated binding energies of O_2 with $Fe_2O_{2,3}^+$ to form ground state $Fe_2O_{4,5}^+$ are only 0.5−0.7 eV (Table 2). $Fe_2O_{2,3}^+$ from $Fe_2O_{4,5}^+$ + N_2 can be interpreted as CID products at E_k greater than 0.5−0.7 eV. The reaction of $Fe_2O_5^+$ with N_2 in the fast flow reactor can produce $Fe_2O_3N_2^+$ (Figure 1), which is supported by the DFT results in Figures 5 and 7. In contrast, $Fe_2O_3N_2^+$ was not observed in the mass selective experiments. This is most possibly because the E_k is

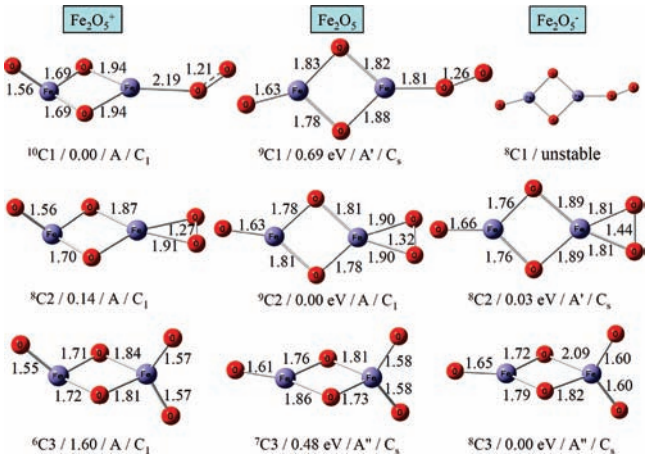

Figure 8. The lowest energy isomers of $Fe_2O_5^q$ ($q = 0, \pm1$) clusters. For each isomer, different spin multiplicities are tested, and the lowest energy structures are listed. See the caption of Figure 3 for explanations.

typically very low (0.13 eV for center of mass approaching velocity of 1 km/s) in the fast flow experiments while E_k can be as large as 1.6 eV in the mass selective experiments.

The major reaction products are $Fe_2O_2^+$/$Fe_2O_2CO^+$ and $Fe_2O_{2,3}^+$/$Fe_2O_3CO^+$ in the reactions of CO with mass selected $Fe_2O_4^+$ and $Fe_2O_5^+$, respectively. Similar to the reactions of $Fe_2O_{4,5}^+ + N_2$, $Fe_2O_{2,3}^+$ from $Fe_2O_{4,5}^+ + CO$ can be interpreted as CID products: $Fe_2O_{4,5}^+ + CO \rightarrow Fe_2O_{2,3} + O_2 + CO$. $Fe_2O_{2,3}CO^+$ may be well interpreted as products from substitution reactions: $Fe_2O_{4,5}^+ + CO \rightarrow Fe_2O_{2,3}CO^+ + O_2$, since the binding of CO with $Fe_2O_{2,3}^+$ should be significantly stronger than that of O_2 and N_2 with $Fe_2O_{2,3}^+$ (Table 2). In addition, $Fe_2O_4^+$ was not observed in the $Fe_2O_5^+ + CO$ reaction, which further suggests that the structure (like $Fe_2O_5^+$/C5 in Figure 3) without the O−O moiety is not the ground state structure of $Fe_2O_5^+$, otherwise the reaction of $Fe_2O_5^+ + CO \rightarrow Fe_2O_4^+ + CO_2$ would produce $Fe_2O_4^+$. It should be pointed out that although the mass selective experimental results have been interpreted based on the PBE calculations in ref 14 a new interpretation of the experiments based on the B3LYP calculations looks more consistent. Additional experimental evidence that supports the existence of the O−O moiety in $Fe_2O_{4-6}^+$ is from the PD experiments, for example, the $Fe_2O_2^+$ fragment was produced from $Fe_2O_6^+$ via the elimination of two units of O_2 upon photon absorption.[26] In conclusion, the CID, PD, and reactivity experiments on $Fe_2O_{4-6}^+$ in the literature[14,26] or in this study can be well interpreted based on the B3LYP calculated ground state structures of $Fe_2O_{4-6}^+$ (Figure 3) that contain O−O unit(s).

4.2. Charge Dependence of Cluster Structures. A previous study of $Fe_2O_{1-5}^-$ clusters by PES has suggested that the ground state structures of anionic $Fe_2O_{4-5}^-$ clusters do not contain a O−O unit.[5] This is in sharp contrast with the conclusion in this study that a η^1-O_2 or η^2-O_2 exists in the ground state of cationic $Fe_2O_{4-5}^+$ (Figure 3). To confirm that the B3LYP/6-311+G* method can correctly predict the ground state of $Fe_2O_5^-$ as suggested by the PES experiments, different structural isomers of $Fe_2O_5^-$ have been optimized. The results along with those of neutral Fe_2O_5[27] and cationic $Fe_2O_5^+$ are given in Figure 8. The $Fe_2O_5^-$/C1 with a η^1-O_2 is unstable and $Fe_2O_5^-$/C2 with a η^2-O_2 is now slightly higher in energy than $Fe_2O_5^-$/C3 without the O−O unit. $Fe_2O_5^-$/C2 and $Fe_2O_5^-$/C3 are close in energy, so the calculation cannot determine if $Fe_2O_5^-$/C3 is the true ground state of $Fe_2O_5^-$. The O−O bond length of the η^2-O_2 in $Fe_2O_5^-$/C2 is 0.144 nm, which is much longer than the bond length (0.121 nm) of free O_2. This means that this O−O bond in $Fe_2O_5^-$/C2 is significantly activated although it is not completely broken. It may be concluded that the B3LYP calculations on $Fe_2O_5^-$ are in agreement with the PES experiments.[5]

The charge dependence of the structures of $Fe_2O_5^q$ ($q = 0, \pm1$) by the DFT in Figure 8 is interesting. The C1 conformer with a η^1-O_2 is the ground state of cationic $Fe_2O_5^+$, the C2 conformer with a η^2-O_2 is the ground state of neutral Fe_2O_5, while the C3 conformer without the O−O unit is the ground state of anionic $Fe_2O_5^-$. As the q of $Fe_2O_5^q$ decreases, the distance between the η^1-O_2 or η^2-O_2 moiety and the host iron atom decreases and the O−O bond length of η^1-O_2 or η^2-O_2 increases. In other words, η^1-O_2 or η^2-O_2 is more strongly bonded and more activated in the cluster system that contains more electrons, which is reasonable as O has high electronegativity.

4.3. η^1-O_2 vs. η^2-O_2. The interesting prediction from the DFT calculations (Figure 3) is that the ground state of $Fe_2O_5^+$ contains η^1-O_2 while the $Fe_2O_6^+$ ground state contains η^2-O_2. This is in parallel with the experimental observation (Figure 1) that $Fe_2O_5^+$ is reactive while $Fe_2O_6^+$ is not reactive toward N_2 and is further supported by the DFT calculations that substitution of η^1-O_2 is easier than that of η^2-O_2 by N_2 (Figures 4−7). Because the substitution of η^2-O_2 in $Fe_2O_5^+$/C2/C4 by N_2 is subject to a small positive (Figure 5) or negative (Figure 7) overall barrier, further investigations such as higher level quantum chemistry calculations are required to confirm the ways of O_2 binding in the ground state of $Fe_2O_5^+$ although the current experimental and DFT studies favor a η^1-O_2 in the ground state $Fe_2O_5^+$.

In the case that the ground state of $Fe_2O_5^+$ is as the DFT calculated ($Fe_2O_5^+$/C1, Figure 3), it is interesting to rationalize why O_2 is end-on bonded in $Fe_2O_5^+$ while side-on bonded in $Fe_2O_6^+$. Normal valence states of the iron element are usually divalent and trivalent in the bulks, e.g., wüstite and hematite, and higher in the intermediates of some enzyme catalytic cycles.[51] The Fe(II) species can be readily oxidized to Fe(III) species while further oxidation of Fe(III) is hard to achieve. With these considerations and the DFT predicted ground state structures in Figures 3 and 8, we may conclude that the way of O_2 binding to Fe(III) is end-on while it is side-on or inserted for the O_2 with iron sites with the valence state being less than +3. The valence state of at least one of the iron atoms in $Fe_2O_2^+$ must be less that +3, so the O_2 is side-on bonded in $Fe_2O_4^+$. For $Fe_2O_3^+$/C1, the net positive charge can be considered to be located mainly on the 2-fold coordinated iron atom (Fe^{2fc}) that is considered to be in the +3 oxidation states, so the O_2 is end-on bonded in the ground state of $Fe_2O_5^+$. The binding of O_2 with the $Fe_2O_2^+$ moiety in $Fe_2O_4^+$ is weak, or at least not as strong, and the binding of a terminal oxygen atom with the $Fe_2O_2^+$ moiety in $Fe_2O_3^+$/C1 (compare reaction 1 with 13 in Table 2), so the electron density around the Fe^{2fc} of $Fe_2O_4^+$/C1 is larger than that around the Fe^{2fc} of $Fe_2O_3^+$/C1. This is supported by the DFT calculated Mulliken charge distribution: +0.939 e on the Fe^{2fc} of $Fe_2O_3^+$/C1 and +0.904 e on the Fe^{2fc} of $Fe_2O_4^+$/C1. As a result, the valence state of Fe^{2fc} of $Fe_2O_4^+$/C1 can be considered to be less than +3 and the O_2 can be side-on bonded in the ground state of $Fe_2O_6^+$.

5. Conclusion

The DFT calculations at the B3LYP/6-311+G* level of theory can reproduce the experimental bond energies of iron oxides with good accuracy. The ground state structures of

$Fe_2O_{4-6}^+$ clusters are predicted to contain O−O unit(s), which is supported by all of the results of CID, PD, and reactivity experiments on $Fe_2O_{4-6}^+$ clusters. Combined with the DFT reaction pathway calculations, reactivity experiments on $Fe_2O_{4,6}^+ + N_2$ in the fast flow reactor conclude that O_2 is side-on bonded in $Fe_2O_{4,6}^+$ clusters. In contrast, both the experiment and theory favor an end-on bonded O_2 in the ground state structure of $Fe_2O_5^+$. The net charge of diiron oxide clusters such as $Fe_2O_5^q$ influences the cluster structures significantly, for example, the O_2 moiety may be end-on, side-on, and inserted bonded in the ground state structures of $Fe_2O_5^+$, Fe_2O_5, and $Fe_2O_5^-$, respectively. For diiron oxides, an O_2 moiety is suggested to be end-on or side-on (or inserted) bonded with iron sites with +3 or less than +3 valence states, respectively.

Acknowledgment. This work was supported by the Chinese Academy of Sciences (Hundred Talents Fund), the National Natural Science Foundation of China (Nos. 20703048 and 20673123), and the 973 Programs (Nos. 2006CB932100, 2006CB806200, and 2006CB403701) of the Ministry of Science and Technology of China.

Supporting Information Available: Tables S1−S6 list the Cartesian coordinates, energies, and vibrational frequencies for all of the optimized structures in Figures 3−8. This material is available free of charge via the Internet at http://pubs.acs.org.

References and Notes

(1) (a) Simándi, L. I. *Dioxygen Activation and Homogeneous Catalytic Oxidation*; Elsevier: Amsterdam, The Netherlands, 1991. (b) Simándi, L. I. *Catalytic Activation of Dioxygen by Metal Complexes*; Kluwer: Dordrecht, The Netherlands, 1992. (c) Simándi, L. I. *Advances in Catalytic Activation of Dioxygen by Metal Complexes (Catalysis by Metal Complexes)*; Kluwer: Dordrecht, The Netherlands, 2003.

(2) Schröder, D.; Fiedler, A.; Schwarz, J.; Schwarz, H. *Inorg. Chem.* **1994**, *33*, 5094.

(3) (a) Bagus, P. S.; Preston, H. J. T. *J. Chem. Phys.* **1973**, *59*, 2986. (b) Engelking, P. C.; Lineberger, W. C. *J. Chem. Phys.* **1977**, *66*, 5054. (c) Green, D. W.; Reedy, G. T. *J. Mol. Spectrosc.* **1979**, *78*, 257. (d) Devore, T. C.; Gallaher, T. N. *J. Chem. Phys.* **1979**, *70*, 4429. (e) Krauss, M.; Stevens, W. J. *J. Chem. Phys.* **1985**, *82*, 5584. (f) Taylor, A. W.; Cheung, A. S.-C.; Merer, A. J. *J. Mol. Spectrosc.* **1985**, *113*, 487. (g) Kröeckertskothen, T.; Knockel, H.; Tiemann, E. *Chem. Phys.* **1986**, *103*, 335. (h) Kröeckertskothen, T.; Knockel, H.; Tiemann, E. *Mol. Phys.* **1987**, *62*, 1031. (i) Andersen, T.; Lykke, K. R.; Neumark, D. M.; Lineberger, W. C. *J. Chem. Phys.* **1987**, *86*, 858. (j) Lee, G.; Oh, S. J. *Phys. Rev. B* **1991**, *43*, 14674. (k) Fan, J. W.; Wang, L. S. *J. Chem. Phys.* **1995**, *102*, 8714. (l) Wang, L. S.; Fan, J. W.; Lou, L. *Surf. Rev. Lett.* **1996**, *3*, 695. (m) Wang, L. S.; Wu, H. B.; Desai, S. R. *Phys. Rev. Lett.* **1996**, *76*, 4853. (n) Drechsler, G.; Boesl, U.; Bäsmann, C.; Schlag, E. W. *J. Chem. Phys.* **1997**, *107*, 2284. (o) Husband, J.; Aguirre, F.; Ferguson, P.; Metz, R. B. *J. Chem. Phys.* **1999**, *111*, 1433. (p) Gutsev, G. L.; Rao, B. K.; Jena, P. *J. Phys. Chem. A* **2000**, *104*, 5374. (q) Aguirre, F.; Husband, J.; Thompson, C. J.; Stringer, K. L.; Metz, R. B. *J. Chem. Phys.* **2003**, *119*, 10194.

(4) Chertihin, G. V.; Saffel, W.; Yustein, J. T.; Andrews, L.; Neurock, M.; Ricca, A.; Bauschlicher, C. W. *J. Phys. Chem.* **1996**, *100*, 5261.

(5) Wu, H. B.; Desai, S. R.; Wang, L. S. *J. Am. Chem. Soc.* **1996**, *118*, 5296. Additions and Corrections: Wu, H. B.; Desai, S. R.; Wang, L. S. *J. Am. Chem. Soc.* **1996**, *118*, 7434.

(6) Yamada, Y.; Sumino, H.; Okamura, Y.; Shimasaki, H.; Tominaga, T. *Appl. Radiat. Isot.* **2000**, *52*, 157.

(7) Cao, Z.; Wu, W.; Zhang, Q. *THEOCHEM* **1999**, *489*, 165.

(8) Gong, Y.; Zhou, M. F.; Andrews, L. *J. Phys. Chem. A* **2007**, *111*, 12001.

(9) Gutsev, G. L.; Khanna, S. N.; Rao, B. K.; Jena, P. *J. Phys. Chem. A* **1999**, *103*, 5812.

(10) Atanasov, M. *Inorg. Chem.* **1999**, *38*, 4942.

(11) Shiroishi, H.; Oda, T.; Hamada, I.; Fujima, N. *Eur. Phys. J. D* **2003**, *24*, 85.

(12) Shiroishi, H.; Oda, T.; Hamada, I.; Fujima, N. *Mol. Simul.* **2004**, *30*, 911.

(13) Reilly, N. M.; Reveles, J. U.; Johnson, G. E.; Khanna, S. N.; Castleman, A. W., Jr. *J. Phys. Chem. A* **2007**, *111*, 4158.

(14) Reilly, N. M.; Reveles, J. U.; Johnson, G. E.; del Campo, J. M.; Khanna, S. N.; Castleman, A. W., Jr. *J. Phys. Chem. C* **2007**, *111*, 19086.

(15) Gutsev, G. L.; Khanna, S. N.; Rao, B. K.; Jena, P. *Phys. Rev. A* **1999**, *59*, 3681.

(16) (a) Abramowitz, S.; Acquista, N.; Levin, I. W. *Chem. Phys. Lett.* **1977**, *50*, 423. (b) Chang, S.; Blyholder, G.; Fernandez, J. *Inorg. Chem.* **1981**, *20*, 2813. (c) Blyholder, G.; Head, J.; Ruette, F. *Inorg. Chem.* **1982**, *21*, 1539. (d) Andrews, L.; Chertihin, G. V.; Ricca, A.; Bauschlicher, C. W. *J. Am. Chem. Soc.* **1996**, *118*, 467. (e) Cao, Z.; Duran, M.; Solà, M. *Chem. Phys. Lett.* **1997**, *274*, 411. (f) Garcia-Sosa, A. T.; Castro, M. *Int. J. Quantum Chem.* **2000**, *80*, 307. (g) Gutsev, G. L.; Rao, B. K.; Jena, P. *J. Phys. Chem. A* **2000**, *104*, 11961. (h) Uzunova, E. L.; Nikolov, G. S.; Mikosch, H. *ChemPhysChem* **2004**, *5*, 192. (i) Uzunova, E. L.; Mikosch, H.; Nikolov, G. S. *J. Chem. Phys.* **2008**, *128*, 094307.

(17) Reilly, N. M.; Reveles, J. U.; Johnson, G. E.; Khanna, S. N.; Castleman, A. W., Jr. *Chem. Phys. Lett.* **2007**, *435*, 295.

(18) (a) Murch, B. P.; Boyle, P. D.; Que, L., Jr. *J. Am. Chem. Soc.* **1985**, *107*, 6728. (b) Rosenzweig, A. C.; Lippard, S. J. *Acc. Chem. Res.* **1994**, *27*, 229.

(19) Shu, L. J.; Nesheim, J. C.; Kauffmann, K.; Münck, E.; Lipscomb, J. D.; Que, L., Jr. *Science* **1997**, *275*, 515.

(20) (a) Cao, Z.; Duran, M.; Solà, M. *J. Chem. Soc., Faraday Trans.* **1998**, *94*, 2877. (b) Jackson, P.; Harvey, J. N.; Schröder, D.; Schwarz, H. *Int. J. Mass Spectrom.* **2001**, *204*, 233. (c) Jones, N. O.; Reddy, B. V.; Rasouli, F.; Khanna, S. N. *Phys. Rev. B* **2005**, *72*, 165411.

(21) Reddy, B. V.; Khanna, S. N. *Phys. Rev. Lett.* **1996**, *93*, 068301.

(22) Schröder, D.; Jackson, P.; Schwarz, H. *Eur. J. Inorg. Chem.* **2000**, *6*, 1171.

(23) Reddy, B. V.; Rasouli, F.; Hajaligol, M. R.; Khanna, S. N. *Fuel* **2004**, *83*, 1537.

(24) Reddy, B. V.; Rasouli, F.; Hajaligol, M. R.; Khanna, S. N. *Chem. Phys. Lett.* **2004**, *384*, 242.

(25) Bacelo, D. E.; Binning, R. C., Jr. *Int. J. Quantum Chem.* **2005**, *105*, 740.

(26) Molek, K. S.; Anfuso-Cleary, C.; Duncan, M. A. *J. Phys. Chem. A* **2008**, *112*, 9238.

(27) Xue, W.; Wang, Z. C.; He, S. G.; Xie, Y.; Bernstein, E. R. *J. Am. Chem. Soc.* **2008**, *130*, 15879.

(28) (a) Asmis, K. R.; Sauer, J. *Mass Spectrom. Rev.* **2007**, *26*, 542. (b) Sierka, M.; Dobler, J.; Sauer, J.; Santambrogio, G.; Brumm̈er, M.; Wo̧ste, L.; Janssens, E.; Meijer, G.; Asmis, K. R. *Angew. Chem., Int. Ed.* **2007**, *46*, 3372. (c) Gruene, P.; Rayner, D. M.; Redlich, B.; Van Der Meer, A. F. G.; Lyon, J. T.; Meijer, G.; Fielicke, A. *Science* **2008**, *321*, 674. (d) Santambrogio, G.; Brumm̈er, M.; Wo̧ste, L.; Dobler, J.; Sierka, M.; Sauer, J.; Meijer, G.; Asmis, K. R. *Phys. Chem. Chem. Phys.* **2008**, *10*, 3992.

(29) Bondybey, V. E.; Smith, A. M.; Agreiter, J. *Chem. Rev.* **1996**, *96*, 2113.

(30) (a) Zhai, H. J.; Kiran, B.; Cui, L. F.; Li, X.; Dixon, D. A.; Wang, L. S. *J. Am. Chem. Soc.* **2004**, *126*, 16134. (b) Zhai, H. J.; Döbler, J.; Sauer, J.; Wang, L. S. *J. Am. Chem. Soc.* **2007**, *129*, 13270. (c) Zhai, H. J.; Wang, L. S. *J. Am. Chem. Soc.* **2007**, *129*, 3022. (d) Zhai, H. J.; Bürgel, C.; Bonacic-Koutecky, V.; Wang, L. S. *J. Am. Chem. Soc.* **2008**, *130*, 9156. (e) Zhai, H. J.; Li, S. G.; Dixon, D. A.; Wang, L. S. *J. Am. Chem. Soc.* **2008**, *130*, 5167.

(31) Geusic, M. E.; Morse, M. D.; O'Brien, S. C.; Smalley, R. E. *Rev. Sci. Instrum.* **1985**, *56*, 2123.

(32) Wang, W. G.; Wang, Z. C.; Yin, S.; He, S. G.; Ge, M. F. *Chin. J. Chem. Phys.* **2007**, *20*, 412.

(33) Frisch, M. J.; Trucks, G. W.; Schlegel, H. B.; Scuseria, G. E.; Robb, M. A.; Cheeseman, J. R.; Montgomery, J. A., Jr.; Vreven, T.; Kudin, K. N.; Burant, J. C.; Millam, J. M.; Iyengar, S. S.; Tomasi, J.; Barone, V.; Mennucci, B.; Cossi, M.; Scalmani, G.; Rega, N.; Petersson, G. A.; Nakatsuji, H.; Hada, M.; Ehara, M.; Toyota, K.; Fukuda, R.; Hasegawa, J.; Ishida, M.; Nakajima, T.; Honda, Y.; Kitao, O.; Nakai, H.; Klene, M.; Li, X.; Knox, J. E.; Hratchian, H. P.; Cross, J. B.; Adamo, C.; Jaramillo, J.; Gomperts, R.; Stratmann, R. E.; Yazyev, O.; Austin, A. J.; Cammi, R.; Pomelli, C.; Ochterski, J. W.; Ayala, P. Y.; Morokuma, K.; Voth, G. A.; Salvador, P.; Dannenberg, J. J.; Zakrzewski, V. G.; Dapprich, S.; Daniels, A. D.; Strain, M. C.; Farkas, O.; Malick, D. K.; Rabuck, A. D.; Raghavachari, K.; Foresman, J. B.; Ortiz, J. V.; Cui, Q.; Baboul, A. G.; Clifford, S.; Cioslowski, J.; Stefanov, B. B.; Liu, G.; Liashenko, A.; Piskorz, P.; Komaromi, I.; Martin, R. L.; Fox, D. J.; Keith, T.; Al-Laham, M. A.; Peng, C. Y.; Nanayakkara, A.; Challacombe, M.; Gill, P. M. W.; Johnson, B.; Chen, W.; Wong, M. W.; Gonzalez, C.; Pople, J. A. *Gaussian 03*, Revision B.05; Gaussian, Inc., Wallingford, CT, 2004.

(34) Stevens, P. J.; Devlin, F. J.; Chablowski, C. F.; Frisch, M. J. *J. Phys. Chem.* **1994**, *80*, 11623.

(35) Sorkin, A.; Iron, M. A.; Truhlar, D. G. *J. Chem. Theory Comput.* **2008**, *4*, 307.

(36) (a) Hay, P. J. *J. Chem. Phys.* **1977**, *66*, 4377. (b) McLean, D.; Chandler, G. S. *J. Chem. Phys.* **1980**, *72*, 5639.

(37) Schlegel, H. B. *J. Comput. Chem.* **1982**, *3*, 214.

(38) (a) Peng, C.; Schlegel, H. B. *Isr. J. Chem.* **1994**, *33*, 449. (b) Peng, C.; Ayala, P. Y.; Schlegel, H. B.; Frisch, M. J. *J. Comput. Chem.* **1996**, *17*, 49.

(39) (a) Gonzalez, C.; Schlegel, H. B. *J. Chem. Phys.* **1989**, *90*, 2154. (b) Gonzalez, C.; Schlegel, H. B. *J. Phys. Chem.* **1990**, *94*, 5523.
(40) Sugar, J.; Corliss, C. Atomic energy levels of the iron period elements: Potassium through nickel. *J. Phys. Chem. Ref. Data* **1985**, 14.
(41) Metz, R. B.; Nicolas, C.; Ahmed, M.; Leone, S. R. *J. Chem. Phys.* **2005**, *123*, 114313.
(42) Hildenbrand, D. L. *Chem. Phys. Lett.* **1975**, *34*, 352.
(43) Huber, K. P.; Herzberg, G. *Molecular Spectra and Molecular Structure: IV. Constants of Diatomic Molecules*; Van Nostrand Reinhold: New York, 1979.
(44) Lias, S. G.; Bartmess, J. E.; Leibman, J. F.; Levin, J. L.; Levin, R. D.; Mallard, W. G. *J. Phys. Chem. Ref. Data* **1988**, *17*, Suppl. No. 1.
(45) Chestakov, D. A.; Parker, D. H.; Baklanov, A. V. *J. Chem. Phys.* **2005**, *122*, 084302.
(46) Loh, S. K.; Lian, L.; Armentrout, P. B. *J. Chem. Phys.* **1989**, *91*, 6148.
(47) Smoes, S.; Drowart, J. *High Temp. Sci.* **1984**, *17*, 31.
(48) Griffin, J. B.; Armentrout, P. B. *J. Chem. Phys.* **1997**, *106*, 4448.
(49) Tan, L.; Liu, F. Y.; Armentrout, P. B. *J. Chem. Phys.* **2006**, *124*, 084302.
(50) Perdew, J. P.; Burke, K.; Ernzerhof, M. *Phys. Rev. Lett.* **1996**, *77*, 3865.
(51) de Oliveira, F. T.; Chanda, A.; Banerjee, D.; Shan, X. P.; Mondal, S.; Que, L., Jr.; Bominaar, E. L.; Münck, E.; Collins, T. J. *Science* **2007**, *315*, 835.

JP810426S